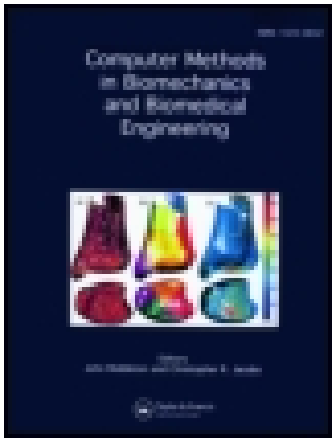

Computer Methods in Biomechanics and Biomedical Engineering

Publication details, including instructions for authors and subscription information:
http://www.tandfonline.com/loi/gcmb20

Numerical investigations of rib fracture failure models in different dynamic loading conditions

Fang Wang[abc], Jikuang Yang[bd], Karol Miller[ce], Guibing Li[fb], Grand R. Joldes[c], Barry Doyle[cg] & Adam Wittek[c]

[a] School of Mechanical and Automotive Engineering, Xiamen University of Technology, Xiamen 361024, China

[b] State Key Laboratory of Advanced Design and Manufacturing for Vehicle Body, Research Centre of Vehicle Traffic Safety, Hunan University, Changsha 410082, China

[c] Intelligent Systems for Medicine Laboratory, School of Mechanical and Chemical Engineering, The University of Western Australia, Crawley-Perth 6009, Australia

[d] Department of Applied Mechanics, Chalmers University of Technology, Gothenburg 41296, Sweden

[e] Institute of Mechanics and Advanced Materials, Cardiff School of Engineering, Cardiff University, Wales, UK

[f] Department of Mechanical and Manufacturing Engineering, Trinity College Dublin, Dublin, Ireland

[g] Centre for Cardiovascular Science, The University of Edinburgh, Edinburgh, UK

Published online: 27 Jul 2015.

To cite this article: Fang Wang, Jikuang Yang, Karol Miller, Guibing Li, Grand R. Joldes, Barry Doyle & Adam Wittek (2015): Numerical investigations of rib fracture failure models in different dynamic loading conditions, Computer Methods in Biomechanics and Biomedical Engineering, DOI: 10.1080/10255842.2015.1043905

To link to this article: http://dx.doi.org/10.1080/10255842.2015.1043905

Computer Methods in Biomechanics and Biomedical Engineering, 2015
http://dx.doi.org/10.1080/10255842.2015.1043905

Taylor & Francis
Taylor & Francis Group

Numerical investigations of rib fracture failure models in different dynamic loading conditions

Fang Wang[a,b,c], Jikuang Yang[b,d]*, Karol Miller[c,e], Guibing Li[f,b], Grand R. Joldes[c], Barry Doyle[c,g] and Adam Wittek[c]

[a]*School of Mechanical and Automotive Engineering, Xiamen University of Technology, Xiamen 361024, China;* [b]*State Key Laboratory of Advanced Design and Manufacturing for Vehicle Body, Research Centre of Vehicle Traffic Safety, Hunan University, Changsha 410082, China;* [c]*Intelligent Systems for Medicine Laboratory, School of Mechanical and Chemical Engineering, The University of Western Australia, Crawley-Perth 6009, Australia;* [d]*Department of Applied Mechanics, Chalmers University of Technology, Gothenburg 41296, Sweden;* [e]*Institute of Mechanics and Advanced Materials, Cardiff School of Engineering, Cardiff University, Wales, UK;* [f]*Department of Mechanical and Manufacturing Engineering, Trinity College Dublin, Dublin, Ireland;* [g]*Centre for Cardiovascular Science, The University of Edinburgh, Edinburgh, UK*

(*Received 8 October 2013; accepted 20 April 2015*)

Rib fracture is one of the most common thoracic injuries in vehicle traffic accidents that can result in fatalities associated with seriously injured internal organs. A failure model is critical when modelling rib fracture to predict such injuries. Different rib failure models have been proposed in prediction of thorax injuries. However, the biofidelity of the fracture failure models when varying the loading conditions and the effects of a rib fracture failure model on prediction of thoracic injuries have been studied only to a limited extent. Therefore, this study aimed to investigate the effects of three rib failure models on prediction of thoracic injuries using a previously validated finite element model of the human thorax. The performance and biofidelity of each rib failure model were first evaluated by modelling rib responses to different loading conditions in two experimental configurations: (1) the three-point bending on the specimen taken from rib and (2) the anterior–posterior dynamic loading to an entire bony part of the rib. Furthermore, the simulation of the rib failure behaviour in the frontal impact to an entire thorax was conducted at varying velocities and the effects of the failure models were analysed with respect to the severity of rib cage damages. Simulation results demonstrated that the responses of the thorax model are similar to the general trends of the rib fracture responses reported in the experimental literature. However, they also indicated that the accuracy of the rib fracture prediction using a given failure model varies for different loading conditions.

Keywords: rib fracture; failure model; thorax; finite element model; dynamic loading

1. Introduction

Thorax injuries rank the second in the overall number of the fatalities and serious injuries in the reported passenger vehicle crashes (Shin et al. 2009) and the severe injury to the thoracic cage is most commonly associated with the rib fractures (Forbes 2005; Li et al. 2010). Therefore, physical tests have been extensively conducted in the vehicle safety field for studies of the fracture tolerance of the rib as well as development of the rib fracture models and criteria. For instance, Granik and Stein (1973) performed three-point bending tests on specimens taken from the sixth and the seventh ribs of the post-mortem human subjects (PMHS) and they reported an average failure von Mises stress of 106 MPa. Charpail et al. (2005) carried out a series of tests under anterior–posterior loading to the intact ribs from PMHS for investigation of the rib mechanical behaviour and fracture threshold. They reported the rib failure strains between 0.0069 and 0.0329. Plank et al. (1998) applied the Mohr–Coulomb yield criterion to investigate the rib failure response using an finite element (FE) thoracic model and they observed that the rib fracture occurs when the von Mises stress reaches 143.4 MPa. Kemper et al. (2005) presented an experimental study using 117 rib cortical bone specimens taken from PMHS at the age ranging from 18 through 67 years. They reported overall average values of the rib failure stress and strain, which are 124.2 MPa and 0.0271, respectively.

Thus, it was noticed that substantial progress has been made for determining the stress and strain that trigger rib fracture, and a number of rib failure models/criteria have been proposed in the literature (Granik and Stein 1973; Plank et al. 1998; Charpail et al. 2005; Kemper et al. 2005). However, the extent of effects of the rib fracture simulation on the thorax injury predictions has not yet been determined in terms of specific uncertainties, including the variations in the rib due to the rib geometry, age of the subject, and so on. The present study was conducted to investigate the biofidelity of the available rib failure models under different loading conditions. The effects of a rib failure model on the responses of a thorax model were investigated under direct impact, which is associated with the loads experienced by a car occupant during an accident. The investigation was performed in two stages in which the FE models increase in complexity from a single rib to a complete thorax:

Stage 1: Investigation of biofidelity of various rib failure and fracture models by simulating the experiments on rib specimens and whole ribs.

*Corresponding author. Email: jikuang.yang@chalmers.se

Stage 2: Analysis of the effects of rib fracture model on prediction of the entire thorax responses to frontal impacts.

2. Materials and methods

The rib fracture failure results from experimental studies were analysed based on the available literature, including rib failure properties from the impact tests using the PMHS rib specimens, and the thorax behaviour and dynamic responses from frontal impact tests on entire thorax. A numerical investigation was carried out using FE models to simulate the rib fracture failure behaviour in the experiments in different configurations, including three-point bending on the rib specimens, the anterior–posterior dynamic loading to an entire bony part of the rib and the frontal impact to an entire thorax at varying velocities.

The performance and biofidelity of the three rib fracture failure models were evaluated with respect to the results from the simulations of the experiments on the rib specimens and the whole ribs. The effects of each rib fracture model on thoracic injury prediction were analysed according to results from the simulations of the thorax response to frontal impacts.

2.1 The configurations of experiments for rib fracture properties

2.1.1 Three-point bending experiment of a rib specimen

Three-point bending is the most commonly used type of loading in the experiments for investigating the biomechanical properties of a human rib (Stein and Granik 1976; Sacreste et al. 1982; Yoganandan and Pintar 1998; Stitzel et al. 2003; Kallieris et al. 2004; Cormier et al. 2005; Mordaka et al. 2007; Tran et al. 2011). In particular, Kallieris et al. (2004) investigated the correlation of rib deflection with respect to the force applied to the rib specimen under quasi-static and dynamic three-point bending. The loadings were imposed using a cylindrical impactor in the direction normal to the rib at velocities of 2 and 4 m/s.

2.1.2 Experiments on a entire rib subjected to anterior–posterior loading

The three-point bending in test of rib mechanical properties represents idealised loading conditions that are unlikely to occur in real-world vehicle crashes. Therefore, a new method was developed to simulate a response to anterior–posterior loading on an entire rib in frontal impact (Charpail et al. 2005). The new method was adapted by Li et al. (2010) in their experimental study for determining the failure and fracture properties of the 2nd, 4th and 10th ribs. In the experiments, the entire bony part of each rib was excised and all soft tissues were removed. Each rib was embedded in a support at the anterior and posterior ends. The ribs were then loaded by displacing the anterior end of the rib towards its posterior end at a constant velocity (1 m/s for the 2nd rib and 0.5 m/s for the 4th and 10th ribs). A single rotational degree of freedom, around an axis normal to the loading plane, was permitted at each end of the rib.

2.2 The configuration of the experiment on thorax frontal impact

The experimental studies on chest frontal impact have been widely conducted to determine the force–deflection behaviour of the human chest and investigate the injury responses of the rib cage (Kroell et al. 1971, 1974; Neathery 1974; Viano 1978; Kent et al. 2003; Kent et al. 2004; Kimpara et al. 2005). It has been suggested in the literature (Kimpara et al. 2005) that the blunt impact test is a better experimental method than the PMHS full-scale sled test when determining the chest stiffness. Therefore, the observed rib fracture results from 38 PMHS frontal pendulum impact tests (Kroell et al. 1971, 1974) were used in this study. Over 70% (27/38) of these tests resulted in at least one rib fracture and 50% (19/38) resulted in more than six rib fractures. In these experiments, the PMHS subjects were positioned in a sitting posture on a flat surface of a rigid table with either a free back or a fixed back. The set-up of the tested thorax with fixed seatback is presented in Table 1. A rigid cylindrical impactor with a diameter of 152 mm and a mass of 10.43 kg struck on the sternum in the mid-sagittal plane at the level of the fourth rib.

2.3 Computational models

A thorax FE model previously developed and validated at Hunan University in a program of human body modelling for vehicle safety (Yang and Yao 2003; Yang et al. 2008; Han et al. 2011; Yang et al. 2013) was used in this study. The geometry of the model was obtained from the computer tomography scans (slice thickness of 1 mm, in plane resolution of 0.25 mm) of an adult male. The body

Table 1. Summary of the PMHS substitutes used in the thorax frontal impact experiments and impact velocity (Kroell et al. 1971, 1974).

Experiment ID	Age	Weight (kg)	Height (cm)	Impact velocity (m/s)
48FM	69	64.4	1.70	7.06
50FM	66	60	1.81	7.29
51FM	60	82.1	1.83	6.66
52FM	65	51.7	1.75	7.2
56FM	65	73.9	1.77	6.93
58FM	68	68.9	1.79	6.75

Table 2. Summary of the rib failure (RF) models.

No.	Failure models	References
RF-Model 1	Mohr–Coulomb yield criterion, failure von Mises stress of 143.4MPa	Plank et al. (1998)
RF-Model 2	Failure effective plastic strain of 0.014	Stitzel et al. (2003)
RF-Model 3	Failure von Mises stress of 124.2 MPa and effective plastic strain of 0.0271	Kemper et al. (2005) and Mordaka et al. 2007

stature is close to the medium size of the American that was used for designing the standard crash dummy.

The thorax FE model was implemented in the explicit dynamics non-linear finite element solver LS-DYNA (version 971) (LSTC 2007). The initial time step was 0.8 μs and the LS-DYNA automated time stepping was used to control the time step during the simulation.

Three rib failure (RF) models were used in this investigation as summarised in Table 2:

- RF-Model 1: The Mohr–Coulomb yield criterion was taken from the study by Plank et al. (Plank et al. 1998). It requires information about the ultimate yield strengths in compression and tension for calculation of the principal stresses.
- RF-Model 2: The von Mises effective plastic strain criterion was used in the study by Stitzel et al. (2003). It has also been used in other FE human body models (Furusu et al. 2001; Li et al. 2010).
- RF-Model 3: The failure criterion uses both the von Mises effective stress and strain that have been derived from the tests using human rib specimens (Kemper et al. 2005; Mordaka et al. 2007).

A matrix (Table 3) was designed for numerical investigation of the effects of the three rib failure models on thoracic injury prediction. All three failure models listed above were investigated for each type of loading on rib and thorax (i.e. three-point bending of a rib specimen, anterior–posterior loading of an entire rib, and frontal impact to the thorax).

2.3.1 *Mesh, loading and boundary conditions for simulation of three-point bending of a rib specimen*

An FE model for simulations of the rib specimen bending tests (Kallieris et al. 2004) is shown in Figure 1. Specific data about the meshes and elements for the specimen FE models of the 6th and the 7th ribs are presented in Table 4. The material properties of the 6th and the 7th ribs were taken from the thorax FE model. An elastic–plastic strain rate-dependent material model is defined for the rib specimen FE models based on available data from the literature (Ruan et al. 2003; Kimpara et al. 2005; Ruan et al. 2005; Mordaka et al. 2007; Shin et al. 2009).

Based on the experimental set-up, each rib specimen model was constrained by two cylindrical supports 0.1 m apart (with contact interface between the rib and support). The rib specimen models were loaded by a rigid cylindrical impactor with a radius of 0.013 m. The impactor was subjected to a velocity of 2 or 4 m/s. The interactions on the interface between the impactor and rib specimen were simulated using a node-to-surface contact model with a friction coefficient of 0.2. The experiments on three-point bending of the 6th and 7th rib specimens (Kallieris et al. 2004) were simulated to evaluate the performance of rib failure model in different loading conditions.

2.3.2 *Mesh, loading, and boundary conditions for simulation of the experiments on a entire rib subjected to anterior–posterior loading*

The responses of the 2nd, 4th and 10th ribs to the test loadings were individually simulated using an entire rib FE model (Figure 2) based on the experiment set-up. The information about the meshes and element types is presented in Table 5. As illustrated in Figure 2, the boundary conditions were defined at the anterior and posterior ends that were constrained by connecting each end to a rigid cap using a revolute joint. A free rotation around the joint is permitted in the loading plane only. The displacements at the anterior end of each rib model were

Table 3. The matrix for investigation of the effects of the rib failure models on the thoracic injury prediction via FE modelling of the experiments.

	Modelling		
Experiments	FE model of test subject	Loading velocity	Number of RF-model
Frontal impact on the thorax	Thorax	6 velocities (Table 1)	1, 2, 3
Three-point bending on a rib specimen	6th and 7th rib specimen	2 m/s and 4 m/s	1, 2, 3
Anterior–posterior loading to a entire rib	419m-Rib 2R, 413m-Rib 4L, and 413m-Rib 10L entire rib	1 m/s and 0.5m/s	1, 2, 3

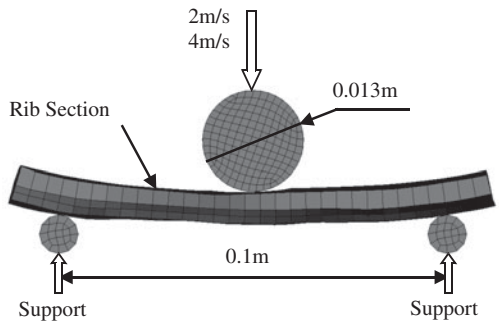

Figure 1. The set-up for FE modelling of the three-point bending experiment on a rib specimen (Kallieris et al. 2004).

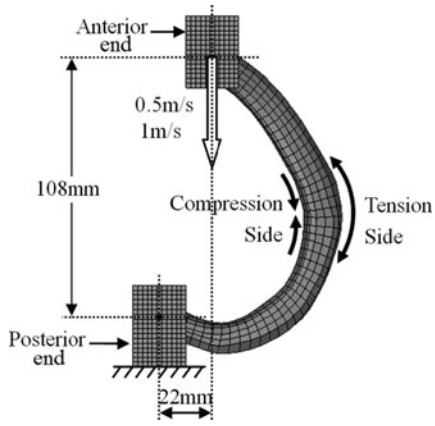

Figure 2. The set-up for FE modelling of the experiment by Zuoping Li et al. (2010) in which the whole ribs (the 2nd rib in this figure) were subjected to a loading in anterior–posterior direction at velocities of 0.5 and 1 m/s.

prescribed at constant velocities of 0.5 or 1 m/s (Li et al. 2010). The resultant joint force at the posterior end of each rib was recorded and compared with the experimental results.

2.3.3 *Mesh, loading, boundary conditions and material properties for the thorax FE model*

The thorax FE model was discretised using both 4-noded rectangular shell elements (Belytschko-Tsay formulation) (Belytschko et al. 1984) and 8-noded constant stress (i.e. with one Gauss point) hexahedral elements (Belytschko and Bindeman 1993) with stiffness-type Belytschko–Flanagan hourglass control (LSTC 2007). The specific details of the complete mesh are presented in Table 6.

As shown in Figure 3, the complete thorax mesh includes ribs, thoracic and abdominal vertebrae, sternum, costal cartilages, internal organs and fat. The vertebra and discs, ribs, costal cartilages and sternum consist of outer cortical bone and inner cancellous bone. Cortical bone was discretised using shell elements while hexahedral solid elements were used for the cancellous bone (Robin 2001; Ruan et al. 2003; Kimpara et al. 2005; Zhao and Narwani 2005; Iwamoto et al. 2007; Mordaka et al. 2007; Shin et al. 2009). The soft tissues were modelled using 8-noded solid elements, including the lungs, heart, liver, spleen, stomach, kidney and fat (Ruan et al. 2003; Kimpara et al. 2005; Ruan et al. 2005; Iwamoto et al. 2007). The ligaments and muscles were modelled with spring elements.

Boundary conditions were defined to replicate the experiments by Kroell et al. (1971, 1974). The back of the thorax model was supported by a rigid wall and a rigid plate was applied to support the bottom of the thorax to ensure that there is no movement of the thorax model in the vertical direction due to the gravity (Figure 4). All the interactions between the body organs and anatomical structures were modelled using frictionless contact interfaces. LS-DYNA automatic surface-to-surface con-

Table 4. Information about element and mesh for the FE models of specimens from the 6th and the 7th ribs.

Rib	Component	Element type	Number of elements	Number of nodes
The 6th rib	Rib trabecular	Solid element (Constant stress)	675	1140
	Rib cortical	Shell element (Belytschko-Tsay)	834	840
The 7th rib	Rib trabecular	Solid element (Constant stress)	476	854
	Rib cortical	Shell element (Belytschko-Tsay)	713	704

Table 5. Information about element and mesh of the FE models of the whole of 2nd, 4th and 10th ribs.

Rib test No.	Component	Element type	Number of elements	Number of nodes
419m-Rib 2R	Rib trabecular	Solid element (Constant stress)	765	1040
	Rib cortical	Shell element (Belytschko-Tsay)	627	632
413m-Rib 4L	Rib trabecular	Solid element (Constant stress)	871	1088
	Rib cortical	Shell element (Belytschko-Tsay)	683	686
412m-Rib 10L	Rib trabecular	Solid element (Constant stress)	366	682
	Rib cortical	Shell element (Belytschko-Tsay)	555	560

Table 6. Summary of anatomy components and mesh of the thorax FE model.

Component	Element type	Number of elements
Vertebra and discs cortical	Shell element (Belytschko-Tsay)	11,698
Rib cortical		15,582
Costal cartilages cortical		3478
Sternum cortical		962
Vertebra and discs trabecular	Solid element (Constant stress)	13,728
Rib trabecular		12,887
Costal cartilages trabecular		3304
Sternum trabecular		1302
Fat		4144
Internal organs		6149
Muscles	Spring element	1043
Ligaments		60

tact formulation was implemented (Zhao and Narwani 2005), which prevents penetration between the organs while allowing for sliding on the interfaces.

Constitutive modelling of the materials in the thorax FE model was implemented by following the literature (Ruan et al. 2003; Kimpara et al. 2005; Ruan et al. 2005; Yang et al. 2006; Mordaka et al. 2007; Shin et al. 2009); an elastic–plastic material model with strain rate dependency was used for the ribs' cortical and cancellous bones and cartilage. The sternum was simulated using the same material properties as the ribs due to the lack of data available in the literature on the sternum. The vertebrae were modelled using a linear elastic material as the vertebral fractures seldom occur due to direct impact to the chest (Kimpara et al. 2005; Shigeta et al. 2009). The constitutive parameters of the bones and cartilage used in the thorax FE model are given in Table 7.

Soft tissues typically behave as hyper-elastic/hyper-viscoelastic nearly incompressible continuum and the parameters for such models have been determined only for a limited number of the abdominal/thoracic organs (Miller

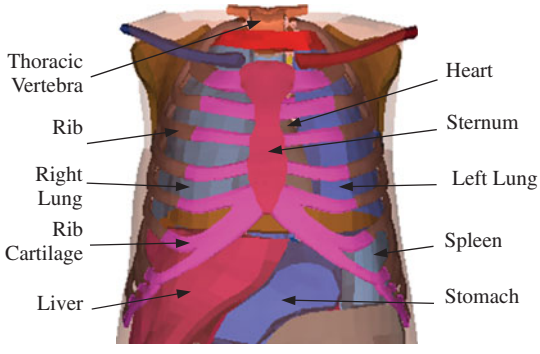

Figure 3. The thorax FE model.

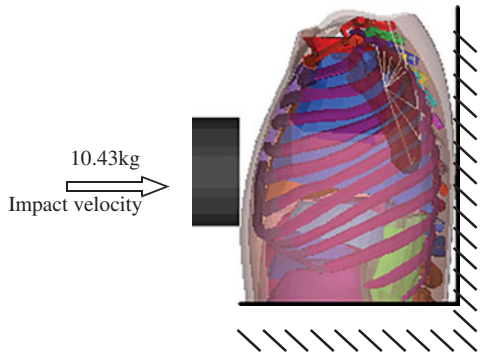

Figure 4. The set-up for FE modelling of the thoracic frontal impact experiments (Kroell et al. 1971, 1974).

2000; Leroy et al. 2001; Schmitt and Snedeker 2006; Gao et al. 2010; Shao et al. 2013). Therefore, a hyper-elastic (Mooney–Rivlin) constitutive model was used for the liver and kidney and a linear viscoelastic constitutive model for the remaining tissues, organs, muscles and ligaments (Lizee et al. 1998; Robin 2001; Ruan et al. 2003; Kimpara et al. 2005; Ruan et al. 2005) (Table 8).

2.3.4 *Validation of the thorax FE model*

The thorax FE model was validated via simulations (Wang et al. 2014; Wang 2014) of volunteer experiments (Patrick 1981) and the PMHS experiments on thoracic frontal impact (Kroell et al. 1971, 1974). For validation using the volunteer experiments, a cylinder (diameter: 152 mm, mass: 10 kg) impacted to the anterior surface of the thorax of a volunteer was simulated at velocities up to 4.6 m/s. For validation against the PMHS experiments, a cylindrical impactor (diameter: 152 mm, mass: 10.43 kg) struck on the thorax was simulated in two groups of loading conditions at velocities up to 8.23 m/s. In the simulations, the force–deflection response to the cylinder impact was reconstructed using the thorax FE model at the same velocities in the experiments. The impactor force was output as a contact load between the impactor surface and the anterior surface of the thorax FE model. Impactor displacement was calculated from node displacement. The thoracic deflection was calculated from changes in the distance between nodes on the anterior and posterior surfaces of the thorax.

Figure 5 demonstrates a comparison of the force–deflection responses between experiments and simulations of the PMHS thoracic impact at velocities of 6.71 to 6.93 m/s (Group 1) and 7.20 to 8.23 m/s (Group 2), which predicts the general behaviour of the force–deflection responses to thoracic frontal impacts at different velocities. The results confirm the capability of the thorax FE model for study of the effects of rib fracture failure models to prediction of thoracic injuries.

Table 7. Material properties of the skeleton components of the thorax model.

Components	Material model	Density (kg/m^3)	E (MPa)	Poison ratio	Yield stress (MPa)	References
Vertebra trabecular	Elastic	1000	1000	0.3		Shigeta et al. (2009)
Vertebra cortical	Elastic	2500	11,000	0.4		Kimpara et al. (2005)
Disc nucleus pulposus	Elastic	1040	2300	0.4		Ruan et al. (2003)
Disc anulus fibrosus	Elastic	1040	300	0.4		Ruan et al. (2003)
Sternum trabecular	Elastic–plastic	1000	40	0.45	1.8	Kimpara et al. (2005) and Yang et al. (2006)
Sternum cortical	Elastic–plastic	2000	10,000	0.3	90	Mordaka et al. (2007)
Rib cartilage trabecular	Elastic–plastic	1000	49	0.4	4.9	Kimpara et al. (2005) and Shigeta et al. (2009)
Rib cartilage cortical	Elastic–plastic	1000	49	0.4	4.9	Kimpara et al. (2005) and Shigeta et al. (2009)
Rib trabecular	Elastic–plastic	1000	40	0.45	1.8	Kimpara et al. (2005)
Rib cortical	Elastic–plastic	2000	10,000	0.3	90	Yang et al. (2006)

Note: E = Young's modulus.

Table 8. Material properties of the soft tissues of the thorax FE model.

Tissues	Material model	Density (kg/m^3)	k (MPa)	Shear modulus G_0 (MPa)	Shear modulus G_i (MPa)	β (decay constant)	References
Heart	Viscoelastic	1000	2.6	0.44	0.15	0.25	Ruan et al. (2003)
Lung	Viscoelastic	600	0.22	0.02	0.075	0.25	Ruan et al. (2003)
Stomach	Viscoelastic	1150	0.145	0.015	0.005	0.635	Ruan et al. (2003, 2005)
Spleen	Viscoelastic	1150	2.875	0.23	0.0436	0.635	Ruan et al. (2005)
Ligaments	Elastic	2000	$E = 20$ MPa				Kimpara et al. (2005)
Muscles	Elastic	900	$E = 0.5$ MPa				Kimpara et al. (2005)
			Hyper-elastic stress parameters				
Liver	Mooney–Rivlin (hyper-elastic)	1040	C10 = C01 = 898 Pa; C20 = C02 = 26,368 Pa; C11 = 0				Miller (2000) and Schmitt and Snedeker (2006)
Kidney	Mooney–Rivlin (hyper-elastic)	1000	C10 = C01 = 6206 Pa; C20 = C02 = 3492 Pa; C11 = 0				Miller (2000), Leroy et al. (2001), and Gao et al. (2010)

Notes: k = bulk modulus, G_0 = short-time shear modulus; G_i = long-time shear modulus, E = young's modulus. C_{ij} ($i, j = 0, 1, 2$): stress parameters of the Mooney–Rivlin model.

Table 9. Comparisons between the experiments (Li et al. 2010) and the simulations of the entire rib responses to an anterior–posterior loading for the fracture time and the corresponding reaction force by means of three rib failure (RF) models.

No. Ribs (donor age)	Model	Rib response data: Fracture time (ms)	Rib response data: Resultant reaction force (N)
419m-Rib 2R (31)	Experiment	18.9	90.7
	RF-Model 1	29.7	156.9
FE model of Rib 2R	RF-Model 2	21.9	142.2
	RF-Model 3	25.9	153.8
413m-Rib 4L (54)	Experiment	82	123.4
	RF-Model 1	140.8	131.8
FE model of Rib 4L	RF-Model 2	108.7	137.3
	RF-Model 3	120.1	136.3
412m-Rib 10L (62)	Experiment	122	87.6
	RF-Model 1	148.9	93.1
FE model of Rib 10L	RF-Model 2	119.6	97.8
	RF-Model 3	135.4	98.9

Note: R, right and L, left.

3. Results

3.1 Results from simulations of three-point bending experiments on rib specimens

For all three failure models, the general behaviour of the predicted force–deflection curves agreed with the experimental results (Kallieris et al. 2004), and the curves (Figure 6) demonstrate the force decrease along with the rib failure fracture.

The results from simulation using RF-Model 3 exhibited slightly better agreement with the experimental data than those from RF-Model 1 and RF-Model 2. However, the differences between the results obtained from the three failure models were within variation of the experimental data. The results for RF-Model 1 and RF-Model 2 can be still regarded as acceptable, as they are within the experimentally determined envelope of rib force–deflection relationship (Figure 6).

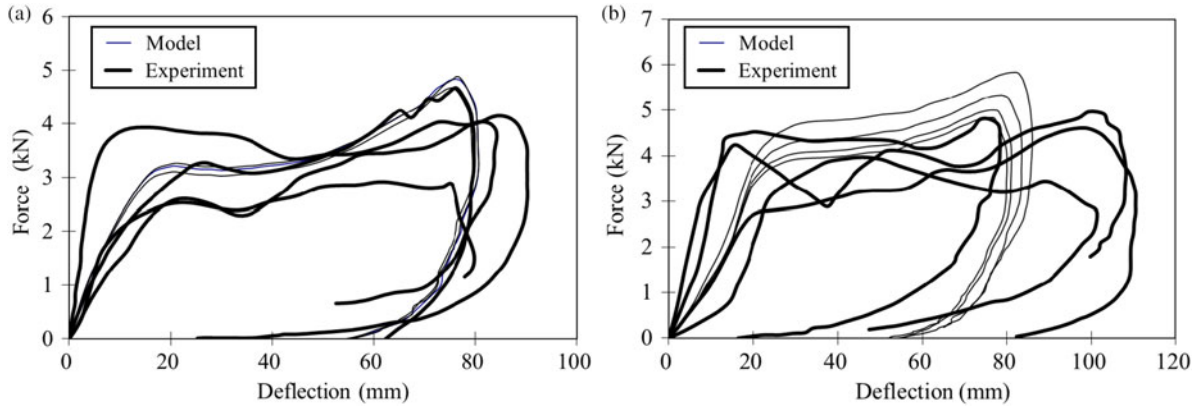

Figure 5. Comparison between the experiments (Kroell et al. 1971, 1974) and the corresponding simulations for the force–deflection responses to thoracic frontal impact: (a) at impact velocities of 6.71–6.93 m/s and (b) at impact velocities of 7.20–8.23 m/s.

3.2 Results from simulations of the anterior–posterior loading experiment on entire rib

The maximum reaction force predicted in the simulations agreed well with the experimental data (Table 9, Figure 7), except for the specimen 419m-Rib 2R. As reported in other studies (Zhou et al. 1996; Li et al. 2010; Vaziri et al. 2010), it was noticed that the rib specimens used by Li et al. (2010) were taken from the PMHS in different age groups. Therefore, one possible explanation for the discrepancies between the modelling and experimental results for specimen 419m-Rib 2R is that our models have not accounted for deterioration of bone strength due to age likely present in the specimens (Li et al. 2010). Table 9 and Figure 7 also indicate that the entire rib FE models tended to overestimate the frequency of rib fractures and the time when the fractures occur.

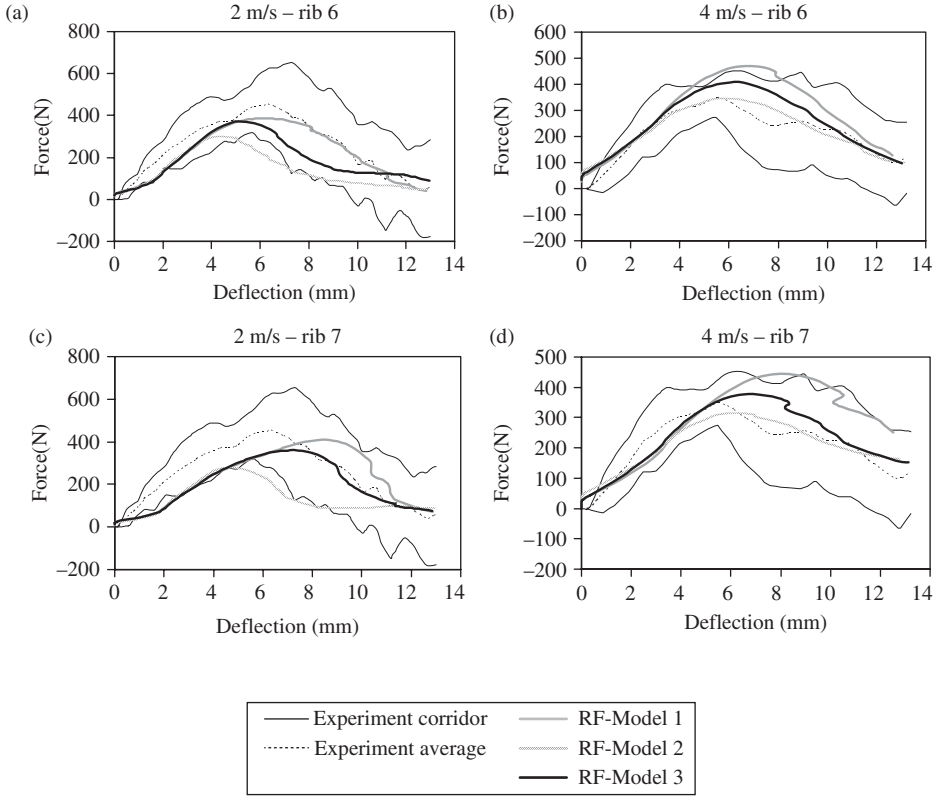

Figure 6. Comparison between the experiments (Kallieris et al. 2004) and the corresponding simulations for the force–deflection responses of the rib specimens taken from the 6th rib (a, b) and the 7th rib (c, d) at impact velocities of 2 and 4 m/s.

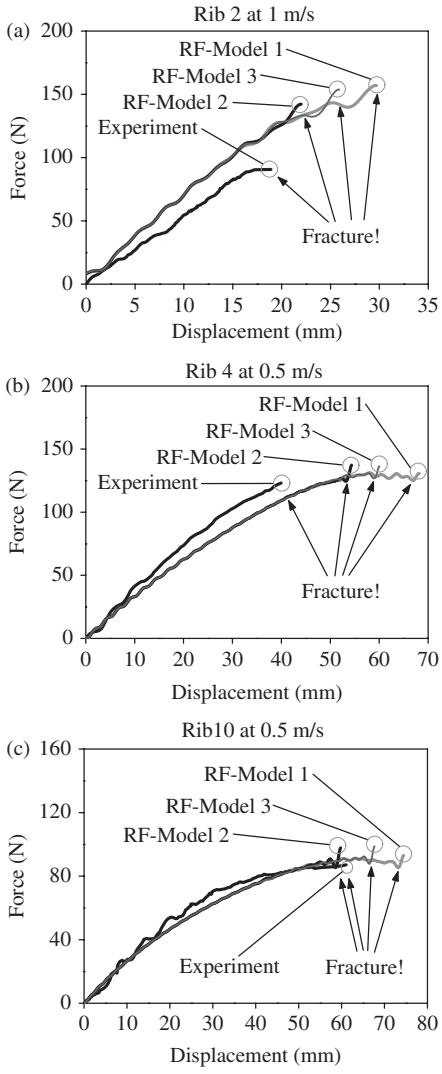

Figure 7. Comparison between the experiments (Li et al. 2010) and the simulations of the force–displacement and fracture responses of the whole ribs: (a) the 2nd rib at 1 m/s, (b) the 4th rib at 0.5 m/s and (c) the 10th rib at 0.5 m/s.

The results from simulations of experiments using PMHS and specimens tend to be affected by inaccuracies and uncertainties when representing boundary conditions and accounting for subject-specific geometry and tissue mechanical properties. Therefore, it could be difficult to determine which of the rib fracture models performs best in terms of variations of the biological subjects, such as human tissues and cadaver specimens. However, the results shown in Figure 6 suggest that force–displacement responses obtained using RF-Model 3 are more close to the experimental results (Li et al. 2010) than the responses from the remaining two RF models.

In simulation of the 413m-Rib 4L test, the rib fracture was predicted at a loading velocity of 1 m/s. The strain distribution on the cross-section of the rib fracture location was analysed by dividing the rib cross-section A-A (Figure 8a) into 12 regions. The six regions (1-6) are allocated at the inner surface of the rib and the other six regions (7-12) at the outer surface of the rib (Figure 8b). The predicted Rib 4L fracture occurred on the inner rib side in the regions 4 and 5, where the calculated effective (von Mises) strain exceeded the rib failure threshold (RF-Model 2) of 0.014. This is consistent with experimental data (Li et al. 2010). In contrast, the predicted maximum effective strain in the regions on the external rib surface was 0.0034, which indicates a very low risk of rib fracture.

3.3 *Results from simulations of thoracic frontal impactor experiments*

Fracture model RF-Model 1 predicted a general increase in the number of rib fractures (NRF) for the impact velocity used in the experiments by Kroell et al. (1971, 1974) (Figure 9). Although fracture models RF-Model 2 and RF-Model 3 also predicted such an increase, they appreciably overestimated the number of rib fractures at low impact velocities.

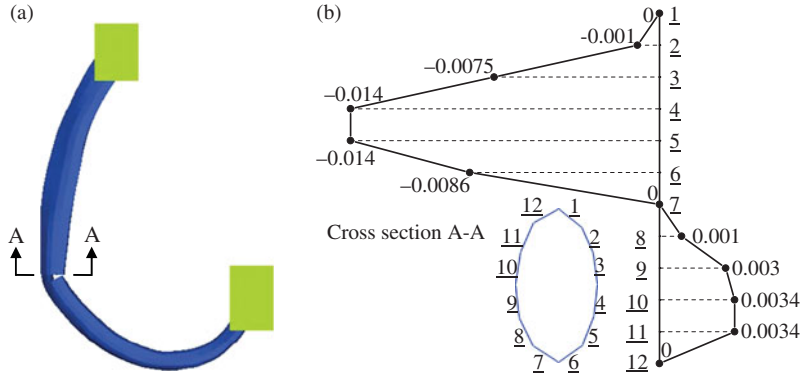

Figure 8. The results from simulation of the entire rib test (Li et al. 2010) on the rib 4L: (a) the predicted fracture location, and (b) the strain distribution on the cross-section of the fracture location (1 through 12 denote regions).

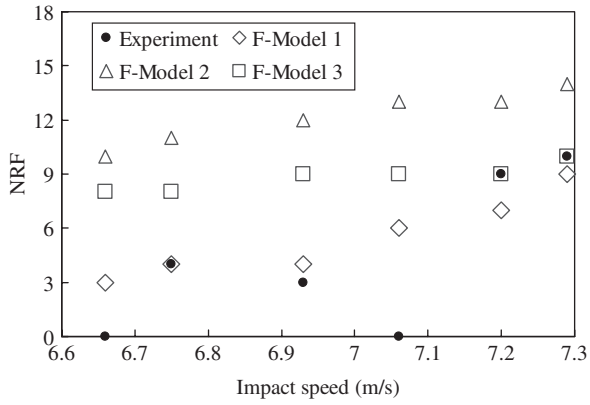

Figure 9. The number of rib fractures (NRF) as a function of the impact velocity determined using results from FE modelling of the thorax impact responses, which is compared with those from experiments on the PMHS thoracic frontal impacts (Kroell et al. 1971, 1974).

4. Discussions and conclusions

In this study, three failure models were applied to predict rib fracture under various loading conditions (Plank et al. 1998; Stitzel et al. 2003; Mordaka et al. 2007). The overall trends of the predicted rib force–deflection responses are acceptable compared with the published experimental data (Figures 6 and 7). However, the results shown in Figures 6, 7 and 9 also indicate that for a given failure model, the prediction accuracy varies appreciably with the loading conditions.

Although it was demonstrated that the rib fracture failure model utilising the Mohr–Coulomb yield criterion (Plank et al. 1998) may be the most suitable one for the simulation using the entire human thorax model, rather than isolated rib models, there were significant differences between the experimental and simulation data at certain impact velocities (Figure 9). This is in contrast to the high biofidelity of the rib models when simulating the experiments on isolated ribs under three-point bending and anterior–posterior loading conditions (Figures 6 and 7). Therefore, the performance of the rib failure models in predicting the failure responses of isolated ribs may not guarantee the predictive effectiveness when modelling the rib responses to actual impacts on the entire thorax.

In the simulations of the experiments on whole ribs, besides the reconstructed fracture location of the test (Li et al. 2010) with the non-uniform strain distribution on Rib 4L (Figure 8), those of the other 2 tests with Rib 2R and Rib 10L also demonstrated non-uniform strain distribution in both the tensile and compression sides. The Rib 4L and Rib 10L failed due to compression, while the rib 2R failed due to tension. It could be attributed to the effect of entire rib geometry on the rib fracture responses. Charpail et al. (2005) and Li et al. (2010) analysed the results from experiments and FE modelling of the rib fractures. They reported that the fracture failures were observed from both sides of the tested rib and they suggested that the rib failure location had a stronger sensitivity to the rib geometry than material law definition, FE model mesh density and variation in bone property. Results from our study also confirmed the observed phenomena by modelling the experimental tests on whole ribs, but there is a limitation for results from simulations with limited rib fracture cases.

It is likely that age variations in the PMHS used previously have influence upon the results. The existing rib failure models, including three models used in this study, do not account for age-related bone strength deterioration, which may affect the results. Future research should investigate the possible role of age in the numerical predictions of rib fracture and development of failure models.

In conclusion, results from this study indicated that the performance of rib failure models in predicting the rib force–deflection responses and fracture location tends to vary for different loading conditions. This suggests that accurate prediction of rib failure may require subject-specific models that take into account the age and geometric differences between individuals involved in different impact conditions.

Acknowledgements

This work was supported by the National Hi-tech Research and Development Program of China (863 Program) under Grant No. 2006AA110101, and the National Natural Science Foundation of China under Grant No. 10472031. The thorax model has been developed as a part of the Human Body Model (HBM) program in Hunan University.

Disclosure statement

No potential conflict of interest was reported by the authors.

References

Belytschko T, Bindeman LP. 1993. Assumed strain stabilization of the eight node hexahedral element. Comput Methods Appl Mech Eng. 105:225–260.

Belytschko T, Lin JI, Tsay C-S. 1984. Explicit algorithms for the nonlinear dynamics of shells. Comput Methods Appl Mech Eng. 42:225–251.

Charpail E, Trosseille X, Petit P, Laporte S, Lavaste F, Vallancien G. 2005. Characterization of PMHS ribs: a new test methodology. Stapp Car Crash J. 49:183–198.

Cormier JM, Stitzel JD, Duma SM, Matsuoka F. 2005. Regional variation in the structural response and geometrical proceedings of human ribs. In: Annual proceedings/ association for the advancement of automotive medicine; Boston, USA.

Forbes PA. 2005. Development of a human body model for the analysis of side impact automotive thoracic trauma [Msater thesis]. Waterloo: The University of Waterloo.

Furusu K, Watanabe I, Kato C, Miki K, Hasegawa J. 2001. Fundamental study of side impact analysis using the finite element model of the human thorax. JSAE Rev. 22:195–199.

Gao Z, Lister K, Desai JP. 2010. Constitutive modeling of liver tissue: experiment and theory. Ann Biomed Eng. 38:505–516.

Granik G, Stein I. 1973. Human ribs: static testing as a promising medical application. J Biomech. 6:237–240.

Han Y, Yang J, Mizuno K. 2011. Virtual reconstruction of long bone fracture in car-to-pedestrian collisions using multi-body system and finite element method. Chin J Mech Eng-En. 24:1045–1055.

Iwamoto M, Nakahira Y, Tamura A, Kimpara H, Watanabe I, Miki K. 2007. Development of advanced human models in THUMS. In: 6th European LS-DYNA users' conference; Gothenburg, Sweden.

Kallieris D, Schönpflug M, Yang J, Ries O, Beaugonin M. 2004. Injury mechanisms database. Official deliverable of HUMOS-2 Report No. 3ESI-030901-E1-DB.

Kemper AR, McNally C, Kennedy EA, Manoogian SJ, Rath AL, Ng TP, Stitzel JD, Smith EP, Duma SM. 2005. Material properties of human rib cortical bone from dynamic tension coupon testing. Stapp Car Crash J. 49:199–230.

Kent R, Lessley D, Sherwood C. 2004. Thoracic response to dynamic, non-impact loading from a hub, distributed belt, diagonal belt, and double diagonal belts. Stapp Car Crash J. 48:495–519.

Kent R, Patrie J, Poteau F, Matsuoka F, Mullen C. 2003. Development of an age-dependent thoracic injury criterion for frontal impact restraint loading. In: 18th international technical conference on the enhanced safety of vehicles (ESV); Nagoya, Japan.

Kimpara H, Lee JB, Yang KH, King AI, Iwamoto M, Watanabe I, Miki K. 2005. Development of a three-dimensional finite element chest model for the 5th percentile female. Stapp Car Crash J. 49:251–269.

Kroell CK, Schneider DC, Nahum AM. 1971. Impact tolerance and response of the human thorax. Stapp Car Crash J. 15:84–134.

Kroell CK, Schneider DC, Nahum AM. 1974. Impact tolerance and response of the human thorax II. Stapp Car Crash J. 18:383–457.

Leroy A, Payan Y, Voirin D, Letoublon C, Troccaz J. 2001. Finite element model of the liver for computer-assisted hepatic tumor ablation. In: Proceeding of BBE.

Li Z, Kindig MW, Kerrigan JR, Untaroiu CD, Subit D, Crandall JR, Kent RW. 2010. Rib fractures under anterior-posterior dynamic loads: experimental and finite-element study. J Biomech. 43:228–234.

Lizee E, Robin S, Song E, Bertholon N, Lecoz J-Y, Besnault B, Lavaste F. 1998. Development of a 3D finite element model of the human body. Stapp Car Crash J. 42:115–138.

LSTC. 2007. LS-DYNA keyword user's manual, version 971. Livermore: Livermore Software Technology Corporation.

Miller K. 2000. Constitutive modelling of abdominal organs. J Biomech. 33:367–373.

Mordaka J, Meijer R, Rooij Lv, Zmijewska AE. 2007. Validation of a finite element human model for prediction of rib fractures. In: SAE world congress; Detroit, USA.

Neathery RF. 1974. Analysis of chest impact response data and scaled performance recommendations. Stapp Car Crash J. 18:459–493.

Patrick LM. 1981. Impact force-deflection of the human thorax. Stapp Car Crash J. 25:471–496.

Plank GR, Kleinberger M, Eppinger RH. 1998. Analytical investigation of driver thoracic response to out of position airbag deployment. Stapp Car Crash J. 42:317–329.

Robin S. 2001. Human model for safety: a joint effort towards the development of refined human-like car occupant models. In: International technical conference on the enhanced safety of vehicles (ESV); Amsterdam, The Netherlands.

Ruan J, El-Jawahri R, Barbat S, Prasad P. 2005. Biomechanical analysis of human abdominal impact responses and injuries through finite element simulations of a full human body model. Stapp Car Crash J. 49:343–366.

Ruan J, El-Jawahri R, Chai L, Barbat S, Prasad P. 2003. Prediction and analysis of human thoracic impact responses and injuries in cadaver impacts using a full human body finite element model. Stapp Car Crash J. 47:299–321.

Sacreste J, Brun-Cassan F, Fayon A, Tarriere C, Got C, Patel A. 1982. Proposal for a thorax tolerance level in side impacts based on 62 tests performed with cadavers having known bone condition. Stapp Car Crash J. 26:155–171.

Schmitt K-U, Snedeker JG. 2006. Analysis of the biomechanical response of kidneys under blunt impact. Traffic Inj Prev. 7:171–181.

Shao Y, Zou D, Li Z, Wan L, Qin Z, Liu N, Zhang J, Zhong L, Huang P, Chen Y. 2013. Blunt liver injury with intact ribs under impacts on the abdomen: a biomechanical investigation. PLoS ONE. 8:e52366.

Shigeta K, Kitagawa Y, Yasuki T. 2009. Development of next generation human FE model capable of organ injury prediction. In: International technical conference on the enhanced safety of vehicles (ESV); Stuttgart, Germany.

Shin J, Untaroiu C, Lessley D, Crandall J. 2009. Thoracic response to shoulder belt loading: investigation of chest stiffness and longitudinal strain pattern of ribs. In: SAE world congress; Detroit, USA.

Stein ID, Granik G. 1976. Rib structure and bending strength: an autopsy study. Calcif Tissue Res. 20:61–73.

Stitzel JD, Cormier JM, Barretta JT, Kennedy EA, Smith EP, Rath AL M DS, Matsuoka F. 2003. Defining regional variation in the material properties of human rib cortical bone and its effect on fracture prediction. Stapp Car Crash J. 47:243–265.

Tran D, Bruyere-Garnier K, Didier AL, Minonzio JG, Foiret J, Vilayphiou N, Talmant M, Laugier P, Mitton D. 2011. Non-invasive assessment of human ribs mechanical properties. Comput Methods Biomech Biomed Eng. 14(sup1):195–196.

Vaziri A, Nayeb-Hashemi H, Akhavan-Tafti B. 2010. Computational model of rib movement and its application in studying the effects of age-related thoracic cage calcification on respiratory system. Comput Methods Biomech Biomed Eng. 13:257–264.

Viano DC. 1978. Thoracic injury potential. In: 3rd international meeting on simulation and reconstruction of impacts in collisions; Bron, France.

Wang F, Yang J, Li G. 2014. Finite element analysis on human thorax responses under quasi-static and dynamic loading. Automot Eng. 36:189–196. (In Chinese with English abstract).

Wang F. 2014. Development of a human thoracic FE model and applied research on thorax injury biomechanics in vehicle impact [Dissertation]. Hunan University, China. (In Chinese with English abstract).

Yang J, Wang F, Li G. 2013. Finite element analysis of thorax responses under quasi-static and dynamic loading. In: Wittek A, Miller K, Nielsen PMF, editors. Computational

biomechanics for medicine. New York: Springer; p. 197–211.

Yang J, Xu W, Dietmar O. 2008. Brain injury biomechanics in real world vehicle accident using mathematical models. Chin J Mech Eng-En. 32:81–86.

Yang J, Yao J. 2003. Development and validation of a human neck FE model in impact loading condition. J Hunan Univ (Nat Sci). 30:40–46. (In Chinese with English abstract).

Yang KH, Hu J, White NA, King AI, Chou CC, Prasad P. 2006. Development of numerical models for injury biomechanics research: a review of 50 years of publications in the stapp car crash conference. Stapp Car Crash J. 50–490.

Yoganandan N, Pintar FA. 1998. Biomechanics of human thoracic ribs. J Biomech Eng. 120:100–104.

Zhao J, Narwani G. 2005. Development of a human body finite element model for restraint system R&D application. In: International technical conference on the enhanced safety of vehicles (ESV); Washington DC, USA.

Zhou Q, Rouhana SW, Melvin JW. 1996. Age effects on thoracic injury tolerance. Stapp Car Crash J. 40:133–144.